MODULATION BY APPLIED ELECTRIC FIELDS OF PURKINJE AND STELLATE CELL ACTIVITY IN THE ISOLATED TURTLE CEREBELLUM

BY C. Y. CHAN AND C. NICHOLSON

From the Department of Physiology and Biophysics, New York University Medical Center, 550 First Avenue, New York, NY 10016, U.S.A.

SUMMARY

1. Quasi steady-state electric fields were applied across the isolated turtle cerebellum to study the relationship between applied field, neuronal morphology and the modulation of the neuronal spike firing pattern.

2. Spiking elements were identified electrophysiologically using extracellular recording methods and by subsequent horseradish peroxidase injection, which revealed their dendritic morphology and orientation.

3. The electric field was precisely defined by measuring the voltage gradients induced in the cerebellum by 40 s constant-current pulses. The field was constant in the vertical (dorso-ventral) axis and zero in the horizontal plane, in agreement with theory.

4. Neurones were modulated by applying a sinusoidal field at frequencies between 0·05 and 1·0 Hz. Modulated cells exhibited an increase in firing frequency and fell into one of four classes, depending on the direction of the field that produced the modulation. Thus neurones were excited by: ventricle-directed fields (V modulation), pia-directed fields (P modulation), both of the above (V/P modulation) or showed no consistent modulation (non-modulation).

5. Most Purkinje somata and primary dendrites (nineteen out of twenty-eight) and most Purkinje dendrites (eighteen out of thirty), were V modulated with maximum rate proportional to the peak field intensity. The dendrites of these cells were consistently oriented toward the pia.

6. Among the stellate cells, the lower molecular layer stellates, with dendrites extending predominantly towards the pia, were mostly (nineteen out of thirty-two) V modulated. The mid-molecular layer stellates, which showed much variability in dendritic orientation, were distributed among all four of the modulation classes. The upper molecular layer stellates, with a mostly horizontal dendritic alignment, were mainly (nine out of sixteen) non-modulated.

7. All groups of spiking elements showed a correlation between patterns of modulation by applied fields and dendritic orientation, which suggests the degree of differential polarization of the extended cable elements of the neurone by the applied field as the basic mechanism for field-induced excitation or inhibition.

8. The threshold for modulation among all neurones was 15–20 mV/mm, which is similar to the fields that modulate other nervous tissues. This suggests that many neurones can be modulated by fields of the order of 10–20 mV/mm.

INTRODUCTION

The processes of a neurone often form a geometric pattern that uniquely characterizes the class to which the cell belongs. When such a neurone is exposed to a constant electric field, potential differences across and currents within the extended cable structures of the cell serve to polarize it differentially and so can change the frequency with which action potentials are generated. The study of this process is important for several reasons. First, it furnishes a powerful method of exploring basic neuronal electrophysiology both at the cellular and local circuit level. Secondly, such studies clarify the possible effects of the intrinsic electric fields that can be generated by the synchronous activity of neuronal ensembles. Thirdly, such investigations have practical applications in the improvement of the design of electric prostheses for the restoration of brain function.

Polarization of neurones and alteration of their activity by applying currents to the brain has been the subject of many previous studies (Brookhart & Blachly, 1952; Terzuolo & Bullock, 1956; Denney & Brookhart, 1962; Landau, Bishop & Claire, 1965; Purpura & McMurtry, 1965; Purpura & Malliani, 1966). A weakness of most of these investigations was a lack of direct measurement of the electric fields actually induced around the target neurones. This was a significant problem because the complex geometry of the preparations, usually areas of the cat brain, very likely resulted in a non-uniform, complex and ill-defined electric field. Another common deficit was the lack of specific cell identification. Recently, much more controlled situations have been studied by using brain slices (Jefferys, 1981; Bawin, Sheppard, Mahoney & Adey, 1984) but the act of creating the slice inevitably alters and reduces the available neuronal circuitry.

The past few years have also seen a renewed interest in the intrinsic field interactions between neuronal populations, particularly as a possible mechanism of seizure propagation (Jefferys, 1981; Jefferys & Haas, 1982; Haas & Jefferys, 1984; Taylor & Dudek, 1984a, b; Taylor, Krnjevic & Ropert, 1984). At the level of the single cell it has long been appreciated that such interactions could occur in appropriately modified systems (Katz & Schmitt, 1940; Arvanitaki, 1942). Examples of such mechanisms have been uncovered also in the specialized axonal cap of the Mauthner cell of fishes (Furakawa & Furshpan, 1963) as well as in related cells (Faber & Korn, 1973; Korn & Faber, 1975). Similar mechanisms also seem to exist in the axonal pinceau of the basket cell of the rat cerebellum (Korn & Axelrad, 1980).

Also of interest is the idea of stimulating specific brain regions, such as the visual cortex (Brindley & Lewin, 1968) to restore partial function, an approach which is beginning to show results in the more peripheral nervous system. Critical to the successful outcome of such a programme is the development of concepts governing the interaction of applied electric fields and neurones, particularly how given neuronal groups may be specifically excited or inhibited.

Our goal in these studies was to apply a simple, well defined, electric field to a population of neurones that comprised distinguishable and identifiable cell types complete with their associated local circuitry and to study the responses of these cells. We used the isolated turtle cerebellum and were able to look at the Purkinje cells

and three distinct classes of inhibitory interneurones, collectively known as stellate cells.

Two main findings emerged; that the major determinant of modulation of neuronal spike activity was the relation between dendritic morphology and the applied field and that the threshold for modulation was remarkably similar amongst all cell classes.

METHODS

Turtles, species *Pseudemys scripta elegans* or *Chrysemys picta* with plastron length 12–15 cm, of either sex, were rapidly decapitated, the skull opened and the cerebellum removed into turtle Ringer solution (NaCl, 100 mM; KCl, 6 mM; NaHCO$_3$, 40 mM; CaCl$_2$, 3·5 mM; MgCl$_2$, 3·5 mM; glucose, 20 mM; bubbled with 95 % O$_2$/5 % CO$_2$). Collagenase (Sigma, Type I) was applied to the pial surface for 10–20 min to aid removal. The pia could also be removed without the enzyme but this increased the risk of damage. No difference in response was seen between the two treatments. All dissections and experiments were carried out at room temperature.

The cerebellum, having the appearance of a flattened ellipsoid, was placed dorsal side up, on a nylon mesh that spanned a hole approximately 9–10 mm in diameter that separated two Plexiglas chambers (Fig. 1). The lower chamber contained a silver plate about 2 cm square and an inlet for Ringer solution. The Ringer solution flowed through the hole separating the chambers, past the cerebellum, and entered the upper chamber where it was removed by suction. A second silver plate could be moved into position in the Ringer solution above the cerebellum. This plate contained a cut-out to enable the recording micro-electrode to be positioned. Both silver plates were chlorided and energized by one of two constant-current systems (i.e. systems that delivered a specified current regardless of any variation in impedance).

The first system was connected to a pulse generator via a photon-coupled battery-powered isolator (WPI Type 305) and generated currents of 0·2–5·0 mA that were applied across the plates for between 20 and 200 s. This system was used in the field-mapping studies. The second constant-current system comprised a completely isolated and battery-powered sine-wave potential generator that fed a similarly isolated constant-current circuit connected to the plates. The sine-wave circuit also generated a reference pulse on each cycle that was emitted, via a photon-coupled isolator, to the recording system to provide a synchronization pulse for the computer when spike-interval histograms were made.

Potentials were recorded with conventional micro-electrodes filled with 3 % horseradish peroxidase (HRP; Boehringer–Mannheim Grade 1) dissolved in 150 mM-KCl and buffered to pH 7·6 with phosphate buffer. The electrode was connected to an active bridge amplifier equipped with a high-current injection circuit. Potentials were recorded against an indifferent electrode made from a Pasteur pipette filled with 4 % agar dissolved in 1 M-KCl and connected with an Ag/AgCl wire.

The viability of the cerebellum was established by monitoring the field potentials evoked by a local surface bipolar stimulating electrode (loc.). Such potentials could be recorded for up to 3 days in this isolated preparation but we usually only recorded for 6–12 h.

Electric field induction and mapping

Before describing the methodology, the basic concept of the design will be clarified. The cerebellum was suspended in the centre of a hole that was significantly larger than the cerebellum itself. Thus most of the applied current bypassed the tissue. There were two reasons for this approach. First, it would be difficult to prevent current leaking around the cerebellum. Secondly, by allowing an extensive extracellular current flow, the influence of the edge of the hole on the field in the tissue was reduced and for theoretical calculations the cerebellum could be represented as being embedded in an effectively infinite medium.

The mapping of the induced fields was accomplished by using a piezoelectric microdrive (Burleigh Inchworm/CE-2000) mounted on a Canberra-type manipulator (Narishige) with micrometer drives on all three axes. The micro-electrode was moved in steps that ranged from 20 to 200 μm while pulses of current were applied between the plates. At each depth the induced potential amplitude during the pulse was measured either with a Nicolet digital oscilloscope (Model 2090) or with a

digital multimeter. The applied current was measured with a battery-powered isolated digital milliammeter. Most measurements were made in the vertical axis near the centre of the preparation but in several series the induced potential was sampled at different locations. At the end of each experiment the micro-electrode was raised above the preparation, the cerebellum removed and the potential measurements repeated in the Ringer solution at the position previously occupied by the tissue. By using an appropriate theoretical expression, the ratio of the conductivity of the cerebellum to that of the Ringer solution could be estimated approximately from these measurements (see Appendix).
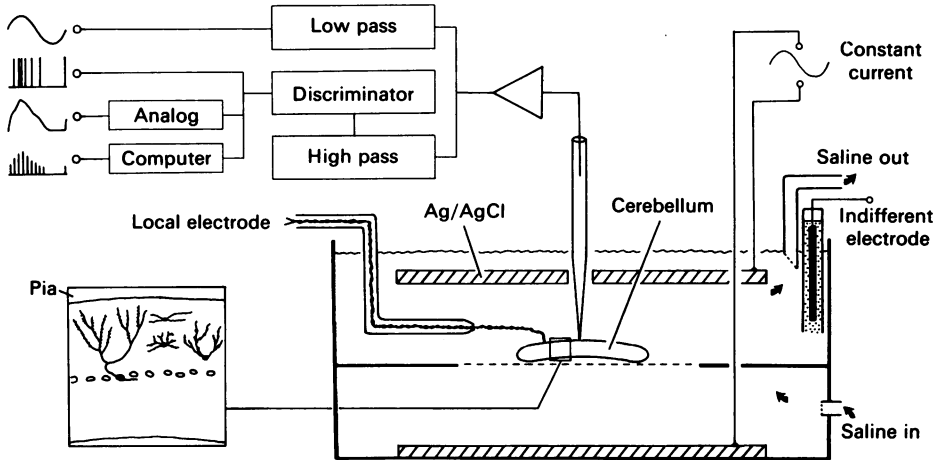

Fig. 1. The stimulating and recording apparatus. The isolated cerebellum rests on a mesh (dotted line) stretched across a hole in the partition separating the upper and lower chamber. Current was passed between the two large Ag/AgCl plate electrodes through the bath and the cerebellum along its dorso-ventral axis. Inset shows orientation of various neuronal elements (see also Fig. 11). The responses recorded from the micropipette were analysed and displayed in various forms represented by the schematic traces on the upper left (see text for details).

Extracellular unit analysis

In these studies a low-frequency sine wave was used to avoid the capacitive membrane currents that are generated with the onset and offset of pulses. The output of the d.c. amplifier connected to the micro-electrode was passed through a low-pass filter (< 25 Hz) and a high-pass filter (> 25 Hz) arranged in parallel (Fig. 1). The signal through the low-pass filter provided continuous monitoring of the quasi-d.c. extracellular potential in the tissue near the tip of the micro-electrode that was generated by the fraction of the applied current that flowed through the cerebellum. This signal was displayed on a chart recorder and also fed through a summing amplifier which added a rectangular synchronizing pulse, phase-locked to the sinusoidal current, to each cycle. This wave form was recorded by an FM tape recorder which simultaneously recorded on a direct channel the spikes from the output of the high-pass filter (see below) for use in later computer analysis.

The spike activities, which were extracted by the high-pass filter, were also fed into a discriminator that generated a pulse for each spike above a selected amplitude. In the turtle cerebellum, where multiple units were very rarely recorded, amplitude discrimination against noise proved to be an efficient method. The pulses were fed directly into a chart recorder as well as via a 2 Hz two-pole low-pass filter, which functioned like a leaky integrator to give a continuous analog histogram of spiking rate. Another channel of the chart recorder displayed the tissue potential from the low-pass filter so that the relationship between the modulation of spiking rate and the sinusoidal field was revealed.

For computer analysis, the spike signals that had passed through the discriminator were fed to the computer. The summed wave form on the FM channel was concomitantly fed to the computer

via an analog-to-digital converter. Spike counting by a clock circuit in the computer was triggered by the synchronizing pulse in each cycle of the summed wave form. Post-stimulus time histograms were accumulated over a selected number of cycles in phase-corresponding bins. Appropriate scaling factors were used to represent instantaneous firing rates at various times (or phase angle) in an average cycle and correlate it with the tissue potential.

Measurement of threshold for modulation

The threshold for modulation was defined as the peak field intensity of the applied sinusoidal field which was just sufficient to cause detectable changes in spontaneous spiking patterns, as discernible from a histogram. These changes included triggering of spiking in silent cells and acceleration or deceleration of the on-going spiking rate in spontaneously active cells. The field intensity was calculated as the product of the threshold current and the electric intensity per unit current determined by field mapping at the end of the experiment.

Identification of the neurones

After extracellular recording we attempted to fill every neurone with HRP. This involved a brief penetration of the neurones using a short burst of negative capacity compensation and subsequent injection of HRP with anodal pulses of 60–90 nA and about 400 ms duration. The penetration was not always successful and the electrode tip usually left the cell after the first few pulses of current injection.

Cerebella containing HRP-filled cells were fixed in Karnovsky fixative for 50 min to a few hours then they were equilibrated in Tris-buffered saline at pH 7·6 and serial parasagittal sections of 75 μm were cut using a Vibratome (Oxford Instruments). Sections were then pre-treated with a filtered mixture of 0·01 % $CoCl_2$ and 0·05 % 3,3′-diaminobenzidine tetrahydrochloride (DAB, Sigma Grade II) at room temperature for 10 min. The mixture was prepared by dissolving 100 mg of DAB in Tris saline buffered so that the final DAB solution was at pH 4·5–5·0. $CoCl_2$ solution was then added while stirring.

After pre-incubation in the DAB–Co^{2+} mixture, 15 ml 0·3 % freshly diluted H_2O_2 was added to the incubation mixture. The tissue was incubated in the solution for 10 min, or until precipitates started to appear at room temperature. The tissue was washed in three changes of Tris-buffered saline for a total of 30 min and then mounted on slides and subsequently dehydrated and cover-slipped.

Electrophysiological characteristics of spontaneous and evoked activities in various HRP-filled neurones were also used for physiological identification of units not filled by HRP.

RESULTS

Viability of preparation

Since the thickness of the entire isolated cerebellum approached 1 mm and most isolated tissues lose viability when their thickness exceeds about 400 μm (Nicholson & Hounsgaard, 1983), we routinely tested the preparation to assess the integrity of the neuronal circuitry.

Loc. stimulation induced typical field potentials (Fig. 2*A*) at all depths. In the series shown the recording electrode entered the cerebellum at the depth indicated as 200 μm. At that level and 25 μm below, a typical early, fast positive–negative potential associated with the presynaptic parallel fibre volley was evident. This component was followed by a well-defined, slower, negativity corresponding to the activation of post-synaptic dendritic elements, assumed to be Purkinje cells (Eccles, Ito & Szentagothai, 1967). These identities were corroborated as recordings were made at deeper levels: the presynaptic potentials rapidly attenuated and the post-synaptic reversed to a positive wave that reached a maximum at 375 μm and then slowly diminished with depth. These potentials are similar to those seen in the cerebellum

of the cat (Eccles *et al.* 1967) and frog (Llinás, 1976); species that exhibit predominantly passive dendritic membrane properties.

The field potentials described above were seen consistently from preparation to preparation and clearly indicated the existence of functional synaptic transmission. Taken together with the multitude of unit recordings to be discussed below, these
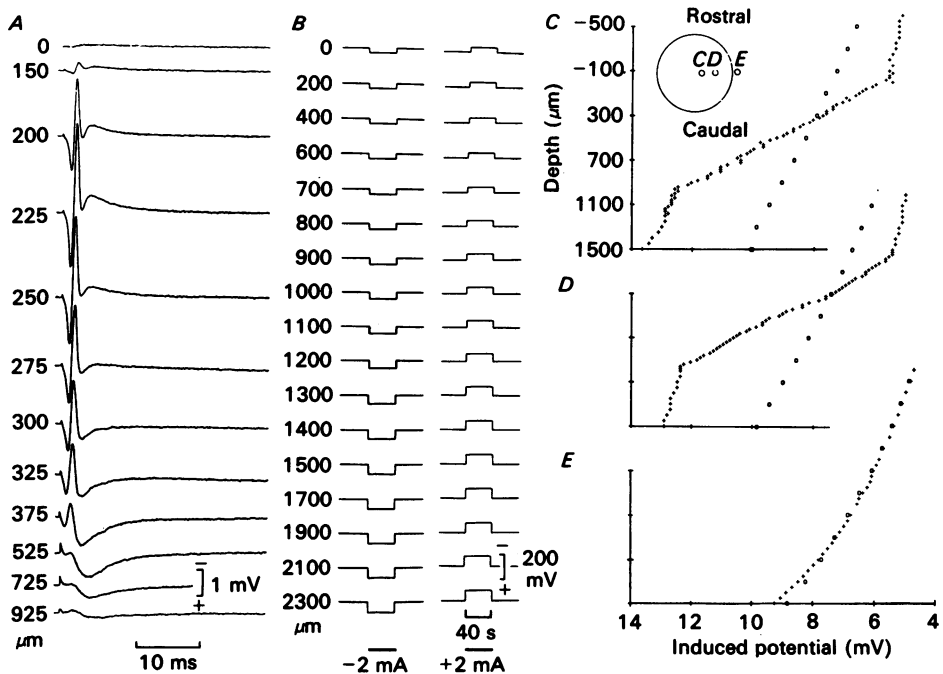

Fig. 2. Depth profile of evoked field potential and mapping of applied current-induced field. *A*, field potential recorded at various depths through the cerebellum evoked by loc. stimulation of parallel fibres. The stimulus artifact can be seen as the first small negativity at deeper levels. The pial surface level is at 200 μm. *B*, potential gradients induced by a square-wave current field applied in the bath in the vertical direction as recorded at various depths above, through and below the cerebellum. Dorsal cerebellar surface at 600 μm, ventral surface at 1500 μm. Polarity of current indicated under Figure. *C*, induced potential difference along track *C* (inset) at various depths (+) and recordings at the same location through the bath with the cerebellum removed ($\bigcirc$). The cerebellum extended from about 0 to 900 μm. *D* and *E*, similar recordings through tracks *D* and *E* (inset). Track *E* lay just next to the cerebellum but the induced field was unaffected by it. Inset in *C* indicating track positions on dorsal cerebellar surface. Track *D* was 1 mm from *C* and track *E* was 2·75 mm from *C*.

data demonstrate the viability of the isolated preparation and confirm the unusual ability of the turtle brain to function in conditions where other tissues would be impaired by anoxia (Lutz, LaManna, Adams & Rosenthal, 1980).

Induced potential mapping

When a long-lasting current pulse was applied between the silver plates, a potential was generated above, below and within the cerebellum (Fig. 2*B*). The magnitude of

the potential induced by the current pulse was a function of the depth of the recording electrode. This potential was subject to an offset that depended on the position of the indifferent electrode, which was constrained by the Plexiglas partition. The relative differences between the potentials recorded at successive depths was the factor that determined the electric field and this was independent of the offset.

Fig. 2C illustrates the induced potentials as a function of depth for an experiment where the potentials were mapped at 25 μm increments ($+$). Potentials induced in the absence of the cerebellum are indicated by a ($\bigcirc$); note the marked difference in slope (inverse of field intensity) in the two cases. The position of the recording electrode track relative to the pial surface is indicated schematically in the inset in Fig. 2E. The first track was close to the centre of the cerebellum while the second (Fig. 2D) was 1 mm lateral to the first. The potentials recorded along the two tracks were very similar, and this uniformity of fields within the cerebellum was confirmed in other mapping experiments. When the potential was recorded outside the cerebellum (Fig. 2E) and 2·75 mm lateral to the original position, the results were very different and the field map coincided with the profile generated in the absence of the cerebellum. This confirmed that the greatly increased conductivity of the bathing medium, relative to the tissue, reduced the perturbing effect of the tissue itself. The lateral displacement of the potential profile in Fig. 2E compared to Fig. 2C, D is due to the proximity of the boundary of the aperture in which the cerebellum resided. It is evident from Fig. 2D, E that the boundary effect was negligible within the cerebellum.

The constant value for the field intensity in a given cerebellum, evident in Fig. 2C, D may appear surprising but in fact the result is predicted by theory as described in the Appendix. Any homogeneous conducting ellipsoid, when placed in a medium of different conductivity and subject to a uniform field, has induced within it another uniform field. The external field, however, becomes non-uniform. This theoretical result, confirmed by measurements, was a major factor in the design of these experiments since it enabled the local field around a neurone to be specified accurately.

As might be expected, the induced fields varied linearly with current in a given experiment over the typical range of currents and the magnitude of the intensity was independent of the polarity of the applied current.

Based on mapping experiments in sixty turtle cerebella we found electric field intensity values ranging from 13 to 43 mV/mm mA and control fields (without cerebellum) from 4 to 9 mV/mm mA. The variations were a function of the chamber used (hole size) and plate position.

Based on eqn. (A 2) in the Appendix and an experimentally determined field intensity ratio (ϵ), a mean conductivity ratio can be calculated, provided that a value is supplied for the ratio a/c of the axes of the ellipsoid representing the cerebellum. We took the average diameter of the turtle cerebellum to be 6·5 mm and the thickness to be 0·9 mm so that the ratio was 7·22. If the ratio of the electric field in the cerebellum, E_c, to that in the bath without the cerebellum (E_0) is defined as $\epsilon = E_c/E_0$ and we take $\epsilon = 3\cdot8$ ($\pm0\cdot1$ s.e. of mean, $n = 60$) then we can obtain a value for k, the ratio of cerebellur tissue conductivity (σ_c) to that of the bathing medium (σ_m) and $k = 0\cdot095$ (see Appendix). This implied that the conductivity of the cerebellum

was some ten times less than that of the Ringer solution. This estimate was subject to considerable uncertainty because there was variation in the geometry of the cerebellum and eqn. (A 2) is quite sensitive to the axis ratio.

Responses and identification of cerebellar neurones to applied low-frequency sinusoidal fields

Frequencies of 0·05–1·0 Hz were applied between the silver plates and the extracellular unit responses recorded from neurones. The identity of the neurone was either revealed by its spontaneous firing pattern and response to loc. stimulation or by penetrating the neurone and injecting HRP which was subsequently visualized by histological processing. Furthermore, the depth of recording was used to aid identification, since HRP-filled neurones showed that the Purkinje somata and the unbranched primary dendrites were typically below 400 μm in depth and the branched dendritic tree above 400 μm, and that stellate cells showed different morphological features at depths above 200 μm, between 200 and 400 μm, and beneath 400 μm. About a third of the neurones from which spikes were recorded (44 out of 130) were filled with HRP. Specifically, 15 out of 33 Purkinje somata or primary dendrites, 10 out of 29 distal dendrites, 13 out of 33 deep molecular layer stellate cells and 6 out of 35 mid and upper molecular layer stellate cells were filled.

We discovered that all the neuronal unit responses could be assigned to one of four modulation classes:

1. V modulation. These cells were excited during the phase when the current was directed toward the ventricle from the pia and inhibited during the opposite phase.

2. P modulation. These cells were excited when the current passed toward the pia from the ventricle and inhibited when the current passed in the opposite direction.

3. V/P modulation. Cells in this category were excited on both of the above current phases.

4. Non-modulation. In some cases, even with a high current strength, the neurones remained unmodulated, or the modulation was erratic, so far as we could tell with the methods used.

Purkinje cells

The morphological characteristics of Purkinje cells were revealed by HRP staining (Figs. 4 A, F; 5 A, G). They were basically similar to those of other species, particularly the alligator and bird (Llinás & Hillman, 1969). An ellipsoidal soma some 30 μm at maximum diameter emitted a thick primary dendrite from one pole and an axon from the other. Often the dendrite ran a considerable distance in the horizontal plane before ascending and bifurcating in the manner characteristic of these cells. The dendritic tree always ramified in the parasagittal plane and was often composed of two to four distinct subtrees, somewhat resembling the Purkinje cells of the elasmobranch (Nicholson, Llinás & Precht, 1969). In other cases the initial dendritic segment ascended directly and then branched progressively.

We divided this cell class into two subcategories: the soma and primary dendrites which we lump together and define operationally as Purkinje cell units encountered below 400 μm beneath the pia, and distal dendrites defined as units of this cell class that lay above 400 μm.

The majority of Purkinje cells were not spontaneously active but were located

either by their response to loc. stimulation or the applied sinusoidal field. Spontan-eously active units showed one of several patterns. Some cells showed very irregular firing (Fig. 3*A*) or irregular bursts within which the spike frequency reached 10 spikes/s (Fig. 3*B*). A few cells showed quite rapid, uneven, spiking at 2–3 spikes/s (Fig. 3*C*). Most spikes were 3–12 mV in amplitude and had a positive–negative form with the two phases of similar magnitude and a total duration of 2–3 ms (Fig. 3*D*).
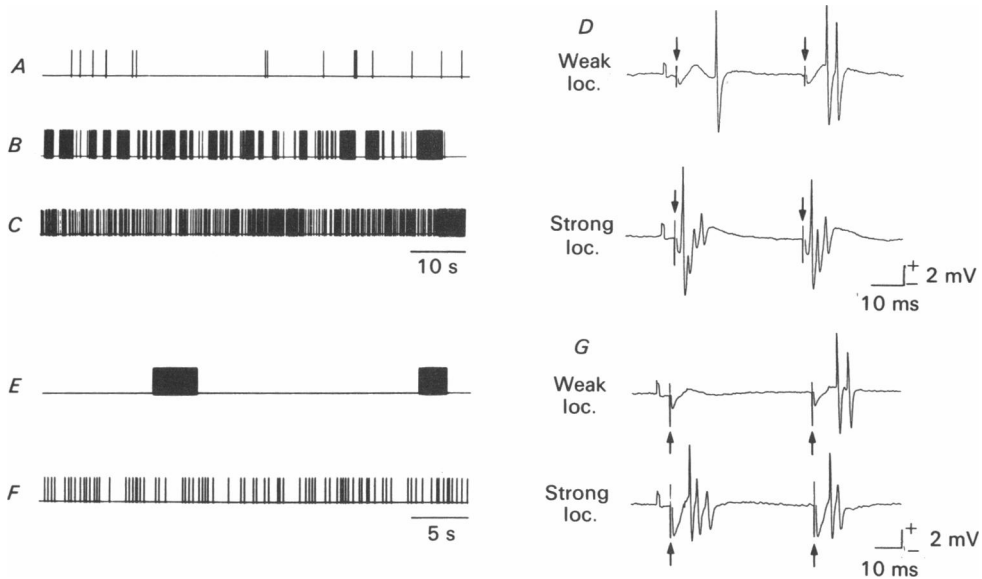

Fig. 3. Spontaneous and loc. stimulation-evoked discharge patterns of Purkinje cell somata and primary dendrites (*A–D*) and distal dendrites (*E–G*). *A–C*, spontaneous discharge patterns of Purkinje cell soma and primary dendrites. *D*, responses to loc. stimulation of parallel fibres (arrows) showing unit spikes superimposed on field potential. Upper trace shows response facilitation by a second identical stimulus. Lower trace shows an enhanced response to increased stimulus strength and reduction in number of spikes evoked by the second stimulus. Unit recorded at 460 μm depth. *E* and *F*, spontaneous discharge of Purkinje cell distal dendrites. *G*, response to double loc. stimulus also showing response facilitation at low stimulus strength and reduction in number of spikes at high stimulus strength despite a reduction in latency. Unit recorded at 370 μm. Time scale in *A*, *B* same as *C*; time scale in *E* same as *F*. Spikes in *A–C*, *E–F* represent standard pulses from discriminator.

Loc. stimulation evoked one or more spikes in a pattern. Stimulation by a weak double loc. stimulus with a separation of 20–70 ms caused an increase in the number of evoked spikes and a reduction in latency for the second stimulus (defined here as 'facilitation') (Fig. 3*D*). At a stronger loc. stimulus, however, a different response pattern consisting of a single large spike followed by a group of small ones was seen (Fig. 3*D*). A second loc. stimulus evoked a reduced number of the smaller spikes (Fig. 3*D*) or a reduced number of spikes of similar amplitude to those evoked by the first loc. Similar depression of spiking in response to the second loc. stimulus at intervals of about 3–50 ms has been reported in cat Purkinje cells and was attributed to the post-synaptic inhibitory action of basket and stellate cells (Eccles, Llinás & Sasaki, 1966*b*). Such depression was not observed at the same intervals in HRP-filled

turtle stellate cells, so its occurrence was used to distinguish Purkinje cells from stellate cells. We define this response depression as 'inhibition'.

Distal dendrites generally showed similar spiking characteristics to the more proximal elements with two patterns predominating. About 60 % of the elements fired in bursts interspersed with long silent periods (Fig. 3E) while most others showed
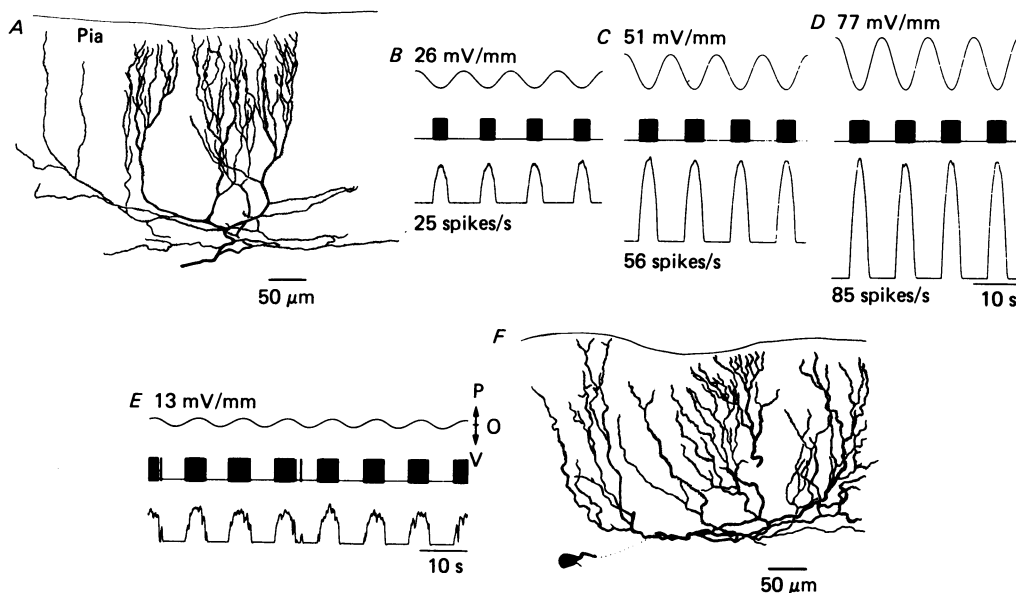

Fig. 4. Modulation of Purkinje cell soma and primary dendrites by applied current field. A, camera lucida drawing of a Purkinje cell injected with HRP at 540 μm. The soma was unfilled. B–D, V-modulation pattern recorded from the unit in A, showing proportionate increase in peak firing rate with increased amplitude of applied field. E, P-modulation pattern observed in one Purkinje cell at 590 μm. F, camera lucida drawing of the unit in E after filling with HRP. The scales in A and F and all subsequent camera lucida drawings have not been corrected for shrinkage (estimated at 30–40 %). In B–E, the three traces represent (top to bottom) (i) applied field with peak values at either polarity stated above the trace, (ii) discriminated extracellular spikes and (iii) analog histogram with peak spiking rate stated below the trace.

slow, irregular spiking (Fig. 3F). Below 150 μm the spike characteristics of the distal dendritic elements were similar to those seen in proximal elements (Fig. 3G). Above that level the spikes were small (about 1 mV). The responses to loc. stimulation (Fig. 3G) were similar to those seen in soma and primary dendrites.

Modulation of Purkinje cells

In nineteen out of twenty-eight Purkinje cell somata and primary dendrites V modulation was seen. All cells showing this type of modulation were also sensitive to the amplitude of the field in that the rate of spiking was enhanced by an increase in field strength (Fig. 4B–D). As shown, the peak spike rate varied in this unit from 25 to 85 spikes/s when the field strength changed from 26 mV/mm to 77 mV/mm in either direction. Analysis of the field strength at which firing commenced, however, revealed that this threshold remained constant at 14 ± 1 mV/mm. Only one soma or

TABLE 1. Threshold and distribution of modulation patterns among Purkinje cells and stellate cells

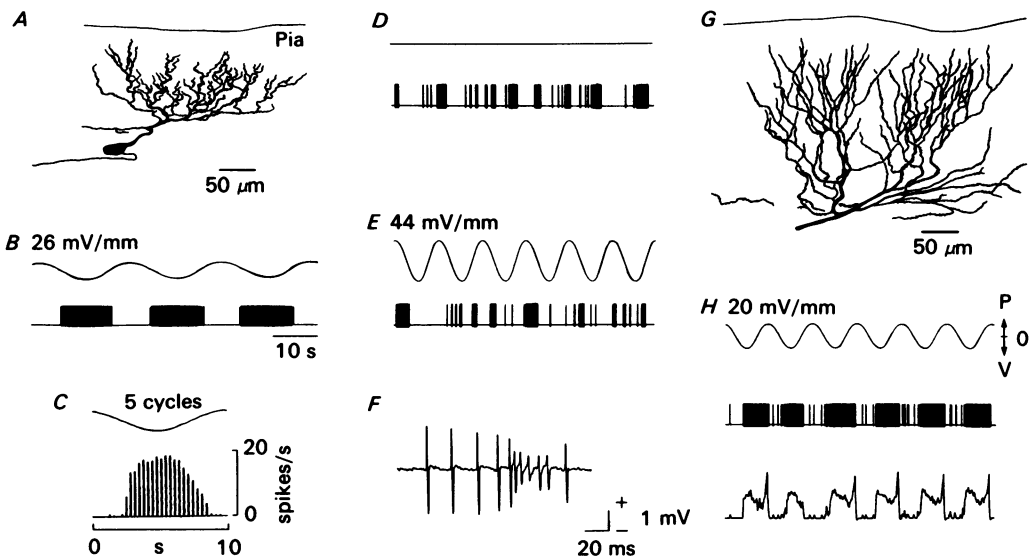| Group	No. of units recorded	Threshold for modulation (mV/mm)				
		All	V	P	V/P	Non
Purkinje cell soma and proximal dendrites	28	15 ± 3 (21)	15 ± 3 (19)	6 (1)	9 (1)	— (7)
Purkinje cell distal dendrites	30	19 ± 2 (22)	20 ± 2 (18)	12 ± 8 (2)	17 ± 4 (2)	— (8)
L.m.s. stellate cells	32	20 ± 3 (28)	21 ± 4 (19)	15 ± 3 (6)	22 ± 3 (3)	— (4)
M.m.s. stellate cells	20	18 ± 2 (14)	18 ± 2 (7)	15 ± 3 (4)	19 ± 4 (3)	— (6)
U.m.l. stellate cells	16	16 ± 3 (7)	22 (1)	7 ± 2 (3)	19 ± 4 (3)	— (9)

Fig. 5. Modulation of Purkinje cell distal dendrites by applied current field. *A–C* illustrate a V-modulated unit (recorded at 400 μm) with the morphology (HRP filled) shown in the camera lucida drawing in *A*, recording of spikes corresponding to the V phase of the applied field in *B* and the rate histogram in *C* showing the instantaneous firing rate at various phases of an averaged cycle. The number of cycles averaged is stated above the histogram. The majority of Purkinje dendrites show V modulation. *D–E* illustrate a unit (depth, 10 μm) in the non-modulated category with *D* showing the irregular spontaneous pattern comprising single spikes and bursts. *F–H* show a V/P-modulated unit at 400 μm. The spikes recorded at the end of each spike train are shown in *F*. The morphology of the cell is shown in camera lucida drawing in *G*. Modulation pattern is shown in *H*. Analog histogram reveals a 'tail-burst' at the end of the spike train. This correlates in time with the pattern shown in *F*. Same time scale in *B*, *D*, *E* and *H*.

proximal dendritic unit showed P modulation (Fig. 4*E*, *F*). Another element of this group exhibited V/P modulation and seven elements were characterized as non-modulated.

The mean threshold for modulation in this group, including V, P and V/P classes, was 15 ± 3 mV/mm ($n = 21$) (Table 1).
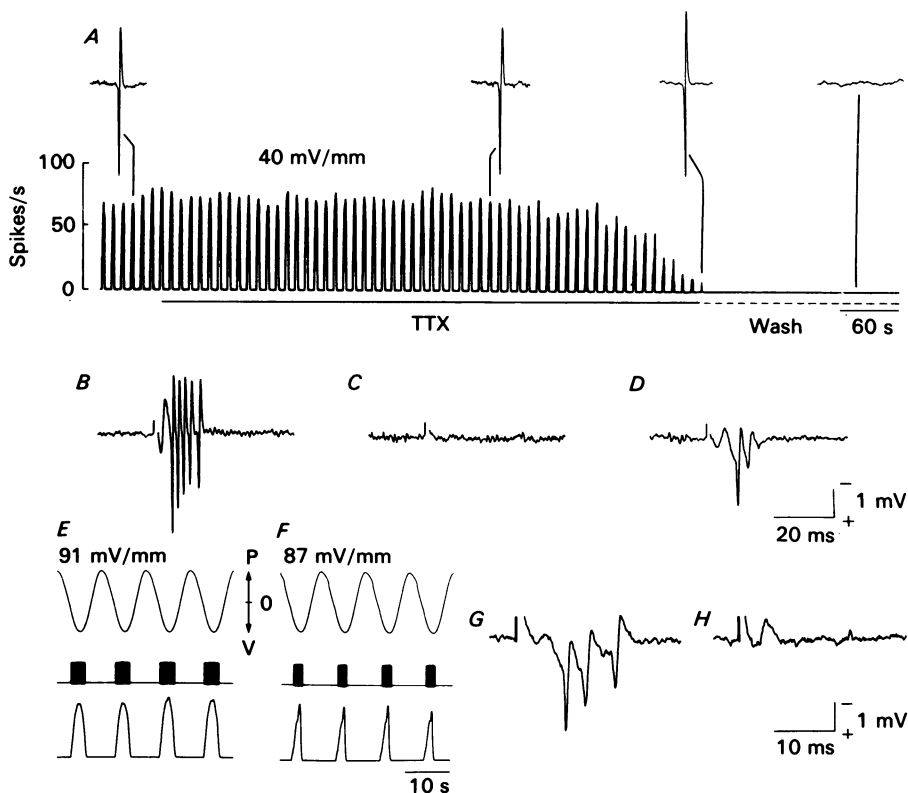
Fig. 6. Effect of TTX (*A–D*) and low-Ca^{2+} Ringer solution (*E–H*) on modulation of Purkinje dendrites by applied field. *A*, continuous analog firing rate histogram of a Purkinje unit recorded at 380 μm in depth. Each deflexion represents the rate of firing during the V phase of an applied sinusoidal field of 40 mV/mm maximum intensity in either direction (not shown). This histogram shows the rates of spiking before, during (continuous line under histogram) and after superfusion of 1 μM-TTX in normal Ringer solution and during wash in normal Ringer solution (dashed line). The applied sinusoidal field was maintained through the wash. The shape of spikes, which was unaffected by the TTX until total blocking, is displayed above the histogram. *B–D*, the loc.-evoked responses before TTX superfusion (*B*), during the first 50 min after total blocking (*C*) and 60 min after total blocking, showing partial recovery (*D*). Time and voltage scales and polarities are identical for all spikes shown. The delay before the commencement of a decline in firing rate was mainly due to the large bath volume (30 ml) and depth of the TTX-sensitive site. *E*, modulation pattern of another Purkinje cell recorded at 400 μm in normal Ringer solution. Field strength = 91 mV/mm. Maximum firing rate = 78 spikes/s. *F*, modulation pattern of same cell as in *E* in Ringer solution containing 0·7 mm-Ca^{2+}, 5·3 mm-Mg^{2+} and 1 mm-Mn^{2+}. Field = 87 mV/mm. Maximum firing rate = 69 spikes/s. *G*, responses to loc. stimulation of same neurone in normal Ringer solution. *H*, loc.-response in the divalent-ion modified Ringer solution showing total blockage of post-synaptic component.

In eighteen out of thirty distal dendritic units, V modulation was observed. Fig. 5*A* shows a Purkinje cell exhibiting this pattern with a typical record in Fig. 5*B* and the histogram in Fig. 5*C*. There was a slowing of the spike burst frequency as it terminated which was seen in a number of cells. Again this modulation pattern showed a strong correlation between applied field intensity and spike frequency. Two units in this group showed P modulation and two showed a tendency to V/P modulation.

Fig. 5*F–H* illustrates one of these units which showed greatest activity at the peak of the V phase. The spiking rate declined gradually and was followed by a renewed acceleration towards a second maximum near the peak of the P phase. Details of the second activation were depicted in Fig. 5*F*, which showed accelerated spiking ending in a rapid burst and subsequent silence. Five units were classified as non-modulated because their irregular firing pattern (Fig. 5*D–E*) persisted during the applied field although some changes of the pattern could be detected.

The threshold for distal dendritic units was 19 ± 2 mV/mm ($n = 22$) for all modulated groups. A more detailed analysis is provided in Table 1. The sodium dependence of the modulated dendritic units was examined in a series of six experiments using 1 M-tetrodotoxin (TTX) in normal Ringer solution. Fig. 6*A–D* illustrates the results in one dendritic unit recorded at 380 μm. The analog histogram in Fig. 6*A* represents the sinusoidally modulated spiking rate of the unit. A few minutes after TTX superfusion, the rate progressively declined to zero. This was typical of the other units tested. The spike amplitude was apparently unaffected until the rate declined to zero (Fig. 6*A*). The response to loc. stimulation before TTX is shown in Fig. 6*B*. After the disappearance of spiking the loc.-evoked response was completely blocked (Fig. 6*C*). Gradual recovery of the loc. response was observed after 60 min of washing in normal Ringer solution (Fig. 6*D*). In another unit, recovery of spiking activated by the applied field was observed.

The possibility that the modulatory effects of the applied field on Purkinje cells were largely the result of a direct modulatory effect on synaptic input was tested in several experiments during synaptic blockage. Fig. 6*E–H* illustrates one such experiment. The modulation pattern was monitored in normal Ringer solution (Fig. 6*E*) and in a low-Ca^{2+} Ringer solution with Mg^{2+} and Mn^{2+} added (Fig. 6*F*). Before applying the field in the low-Ca^{2+} Ringer solution, synaptic blockage was tested by stimulation and showed complete blockage of the response to peduncle stimulation (not shown) and of the spikes and the later components of field potential in response to parallel fibre stimulation (Fig. 6*H*; control in Fig. 6*G*). There was no blockage of modulation by the field. Some minor changes in the modulation pattern were seen which may be attributed to excitability changes caused by alteration of divalent ion content of the Ringer solution.

Stellate cells

The interneurones of the molecular layer could be divided into three subclasses: lower, mid and upper molecular layer stellate cells. Within each class a distinct morphology was evident in the orientation of the dendrites.

The lower molecular layer stellates (l.m.s.) were located between 400 and 500 μm with their somata close to those of the Purkinje cells. The cell bodies of the l.m.s. were smaller than those of the latter cell type and often shaped like an inverted triangle with dendrites leaving two basal vertices and an axon emerging from the apex. In some cases axons emerged from dendrites and on occasion it appeared that these cells emitted axons from multiple sites. The dendrites ascended toward the pia and so these stellates showed a distinct anatomical polarization resembling that of Purkinje cells. The dendrites tended to be beaded and lacked prominent spines while the axons also showed fine beads and ramified in all directions (Fig. 8*C, F*).

Most l.m.s. fired regular, spontaneous spikes at 2–5 spikes/s (Fig. 7*A*) while others

showed a much faster firing rate (Fig. 7B) or a more irregular pattern (Fig. 7C–D). Spikes were typically 1–3 mV in amplitude and positive–negative, with the positive phase predominating (Fig. 7G). Loc. stimulation typically evoked a single spike while double loc. stimulation increased the number but never reduced it (Fig. 7G).
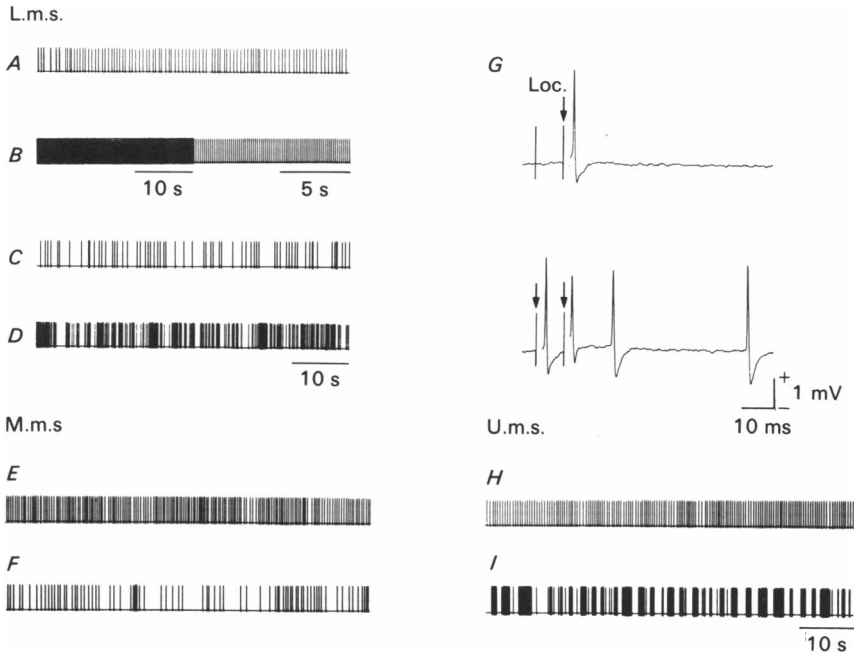

Fig. 7. Spontaneous spiking patterns of stellate cells l.m.s. (A–D), m.m.s. (E–F) and u.m.s. (H–I) units, and loc.-evoked pattern typical of all three classes of stellates (G). Upper trace in G: response to a loc. stimulation of parallel fibres (arrow). Lower trace: response to two closely spaced identical loc. stimulations. The unit in G was recorded at 550 μm. Spikes in A–F, H, I represent pulses from discriminated unit. Time scale in A is same as that for left-hand side of B. Time scales in C same as for D, and time scale for E, F and H same as for I.

Mid-molecular layer stellates (m.m.s.) lay between 200 and 400 μm and exhibited the greatest morphological diversity amongst the stellate class. While the dendrites of some cells were clearly polarized toward the pia, other cells showed a true stellate morphology with dendrites oriented in all directions while yet others displayed a predominantly horizontal organization (Fig. 9A, D, G).

Most m.m.s. fired evenly at 2–3 spikes/s (Fig. 7E) but others were somewhat less regular (Fig. 7F). Responses to loc. stimulation resembled those for the l.m.s.

Upper molecular layer stellates (u.m.s.) were found in the first 200 μm below the pia. These cells were predominantly horizontal in their dendritic morphology and had a smaller soma than the cells lower down (Fig. 10C, E). They usually had a spontaneous firing pattern at about 30 spikes/s (Fig. 7H) but a few showed irregular high-frequency bursts (Fig. 7I). Again the responses to loc. stimulation were similar to those of the other classes of stellate cell.

Modulation of stellate cells

As shown in Table 1, the majority (nineteen out of thirty-two) of l.m.s. were V modulated (Fig. 8 *A–F*). Although the extent of the modulation was less than that seen in Purkinje cells, it was still evident from visual inspection of the record. Six
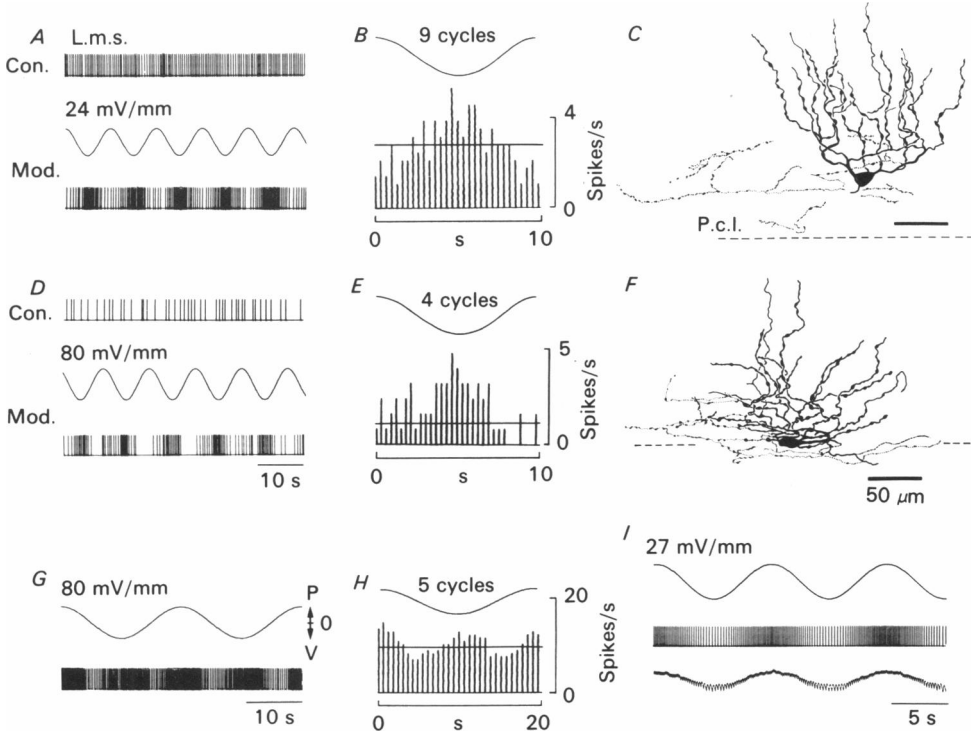

Fig. 8. Modulation pattern of l.m.s. units. *A*, discriminated spikes recorded from a stellate cell at 450 μm firing spontaneously (con.) and during application of a current field (mod.) showing V modulation by the applied field (middle trace) the peak amplitude of which is stated above the trace. *B*, firing rate histogram of the spikes in *A* averaged over 9 cycles. The horizontal line indicates mean spontaneous firing rate. *C*, camera lucida drawing of the unit in *A* and *B* after filling with HRP. Fine dotted lines represent axons. P.c.l. = Purkinje cell layer. *D–F*, similar illustration of spikes, rate histogram and camera lucida drawing of another V-modulated l.m.s. unit recorded at 400 μm. *G–H*, spikes and firing rate histogram of an l.m.s. unit recorded at 420 μm showing V/P modulation. *I*, spikes and analog histogram (middle and bottom traces, respectively) of an l.m.s. unit recorded at 550 μm showing P modulation by the applied field (top trace). Time scale in *D* applies to *A*. Length bar in *C* represents same distance as in *F*.

out of the thirty-two cells were P modulated (Fig. 8 *I*) and three were V/P modulated (Fig. 8 *G*, *H*). Four units were assigned to the non-modulated category.

Amongst the m.m.s, V modulated units still constituted a majority class with seven candidates out of twenty units recorded (Fig. 9 *A–C*). Three m.m.s. units were classified as P modulated while three showed V/P modulation (Fig. 9 *D–F*). The V/P pattern was apparently distinct from the V/P modulation in Purkinje cell units in that the P-phase activation did not appear to be associated with extended spiking

past the peak of the V phase. Five cells were non-modulated; one example is shown in Fig. 9G–I.

In the u.m.s. class, the largest unit class contained those described as non-modulated, having nine out of sixteen examples (Fig. 10A–E). Only one unit showed V
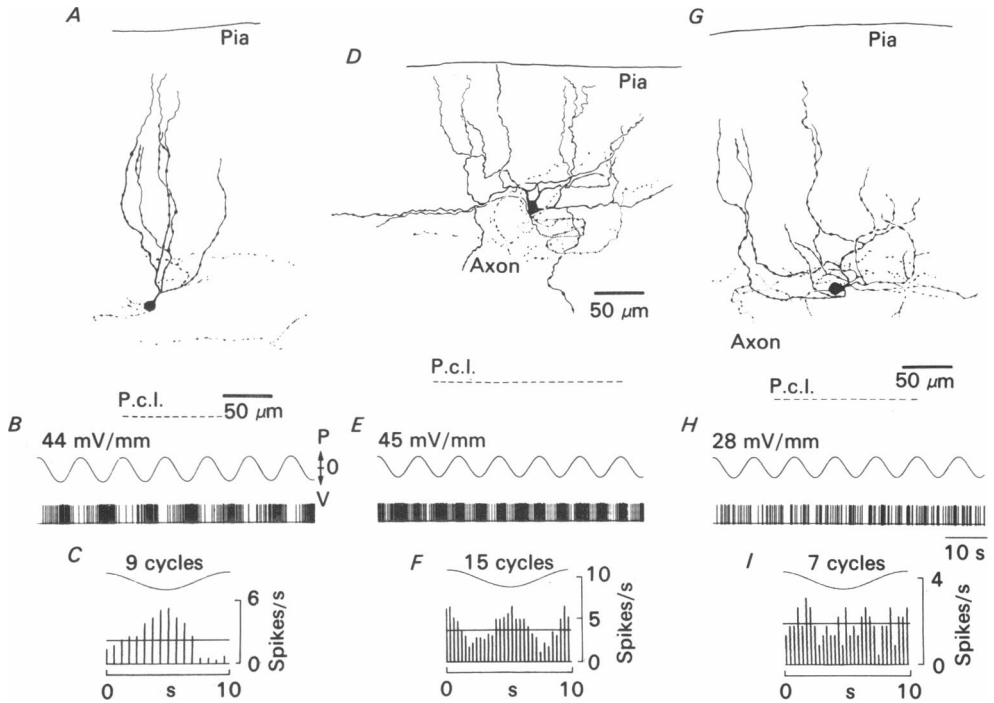

Fig. 9. Morphology and modulation pattern of m.m.s. units. *A–C*, camera lucida drawing, spikes under modulation and firing rate histograms illustrating an m.m.s. unit recorded at 350 μm showing V modulation. *D–F*, morphology, spikes under modulation and firing rate histogram of an m.m.s. unit recorded at 240 μm showing a V/P modulation pattern. *G–I*, morphology, spike activities during application of current field and firing rate histogram of a non-modulated m.m.s. unit recorded at 260 μm. Fine dotted lines in the camera lucida drawings represent axons. P.c.l. = Purkinje cell layer. The line across each histogram represents mean spontaneous firing rate. Time scale in *H* applies to *B* and *E*.

modulation while three showed P modulation (Fig. 10G) and three showed some degree of V/P modulation, such as the unit shown in Fig. 10F.

The thresholds for modulation of l.m.s., m.m.s. and u.m.s. were 20 ± 3 mV/mm ($n = 28$), 18 ± 2 mV/mm ($n = 14$) and 16 ± 3 mV/mm ($n = 7$) respectively.

DISCUSSION

The conclusion to be presented in this Discussion is that the degree and type of modulation of Purkinje and stellate cells is simply explained in relation to the direction of the applied field and the dendritic geometry. In turn this suggests that modulation is directly related to the extent of the polarization induced in the extended dendritic cable structures of the neuronal dendrites.

Characteristics of induced field

A key premise of these studies was that the induced field within the cerebellum was constant. This result was both predicted on theoretical grounds (Appendix) and demonstrated experimentally.
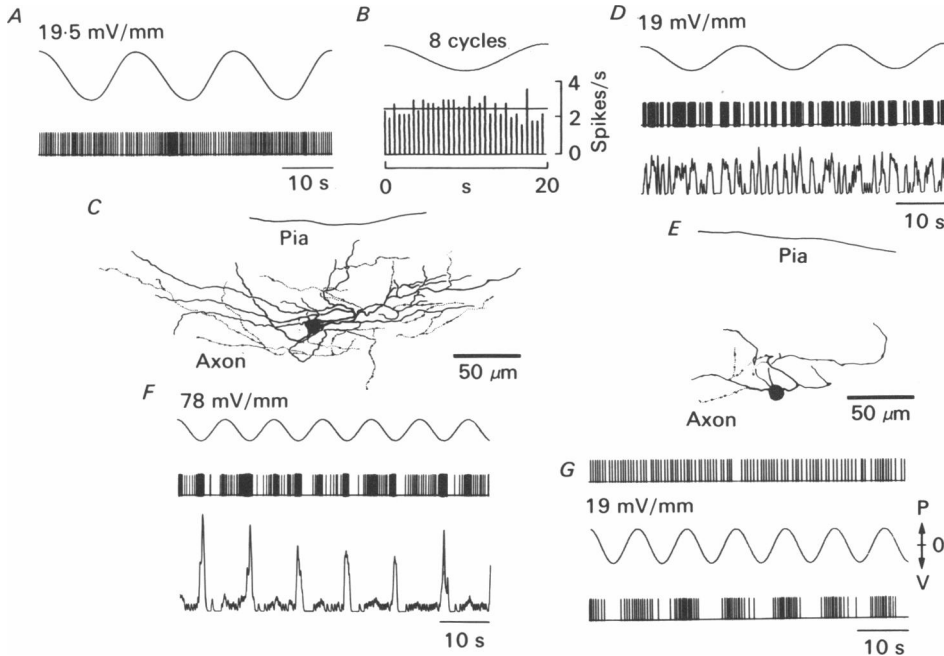

Fig. 10. Modulation of u.m.s. units. *A–C*, spikes during application of current field (*A*), firing rate histogram (*B*) and camera lucida drawing (*C*) of an HRP-filled unit in the non-modulated category recorded at 120 μm. Horizontal line in histogram represents mean spontaneous firing rate. *D*, *E* illustrate another non-modulated m.m.s. unit recorded at 150 μm. *D*, spikes and bursts recorded during application of current field. Bottom trace shows the analog histogram of the spiking pattern. *E*, camera lucida drawing of the unit in *D* after HRP filling (filling probably very incomplete). *F*, V/P modulation pattern illustrated in a u.m.s. unit recorded at 170 μm. Top trace: current field applied. Middle trace: spikes during application of field. Bottom trace: analog histogram of the spikes showing dual-phase excitation. *G*, P modulation illustrated in a unit recorded at 140 μm. Top trace: spontaneous spiking pattern. Middle and bottom traces: applied field and modulated spiking pattern.

Our field measurements indicated the absence of an induced field in the horizontal plane within the cerebellum. We did not detect any non-homogeneity in the *z*-axis despite the different cytoarchitectonic characteristics of molecular, Purkinje and granular layers. This finding was consistent with earlier studies in frog and toad (Nicholson & Freeman, 1975) and recent studies in the rat cerebellum based on diffusion analysis (Nicholson & Phillips, 1981). Some difference was reported in cat cerebellum, however (Yedlin, Kwan, Murphy, Nguyen-Huu & Wong, 1974).

The application of steady electric currents across assemblies of oriented core conductors is known to produce changes in extracellular K^+ concentration ($[K^+]_o$) due to the selective movement of K^+ across the membranes of certain cells, most

probably glia (Gardner-Medwin, 1983; Gardner-Medwin & Nicholson, 1983). Since changes in $[K^+]_o$ can influence neuronal excitability this could lead to changes in the firing pattern of cells. In a separate study we examined this effect in the turtle and found that in a period of 5 s at the typical field strengths used here, the increase or decrease in $[K^+]_o$ did not exceed 1 mM (C. Nicholson, unpublished observations).
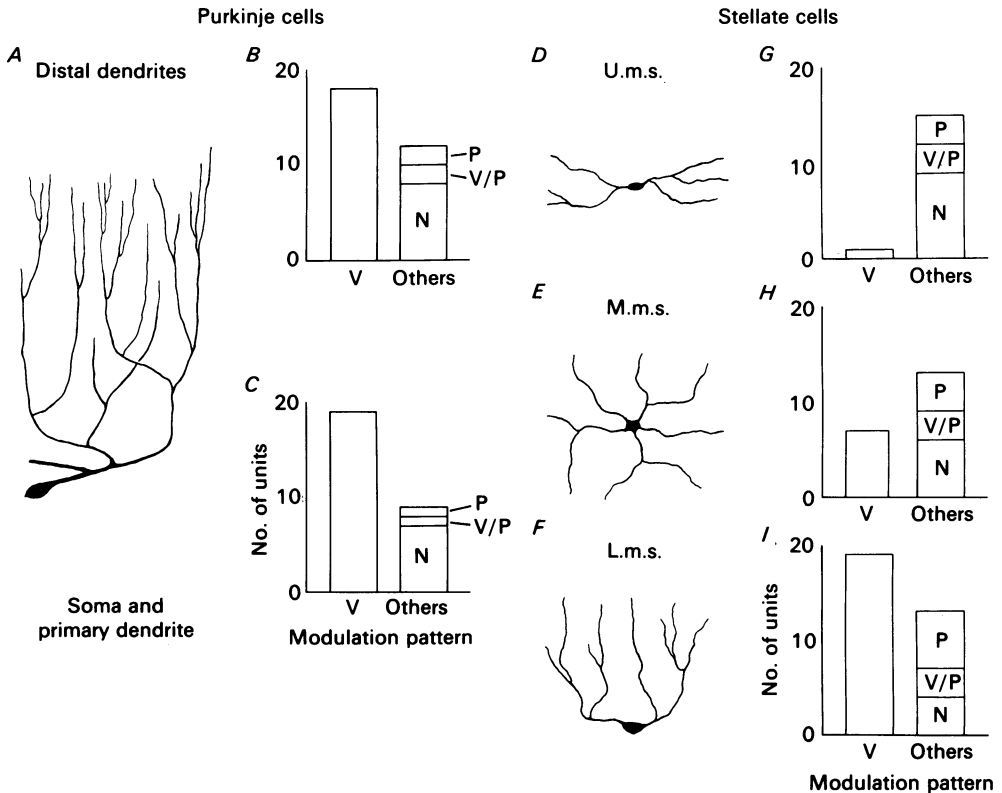

Fig. 11. Summary of dendritic orientation *vs.* modulation pattern in the various cerebellar neuronal elements. Schematic representation of typical orientations of dendrites in various neuronal elements are presented in *A*, *D*, *E* and *F* against the histograms in *B*, *C*, *G*, *H* and *I* that show the distribution of modulation patterns among units in the respective morphological groups. The label N represents non-modulated units. See Table 1 for details.

Since our normal Ringer solution contained 6 mM-K^+, such changes would be unlikely to have much influence on the neurones. Any effect would also be further diminished by the fact that a sinusoidal field was used with a maximum period of 20 s.

Modulation of Purkinje cells

As seen from Table 1 and Fig. 11, the majority (thirty-seven out of fifty-eight) of all Purkinje cell elements recorded were excited by current directed from pia to ventricle. Characteristically, such units either remained silent or the spontaneous activity was totally inhibited for current flow in the opposite direction. Very few

elements were excited by pia-directed current (three out of fifty-eight) or by both polarities (three out of fifty-eight). A total of fifteen cells were classified as non-modulated; this included cells where some effect was seen but the effect was too subtle and irregular to be easily characterized.

Since all Purkinje cells have dendritic trees that are strongly oriented in the vertical direction, the modulation results are quite consistent with the concept that current passage that tends to depolarize the soma leads to excitation while current of the opposite polarity hyperpolarizes the soma and leads to inhibition of firing. The minority of cells that did not conform to that pattern could be damaged, either by the micro-electrode or due to the inevitable trauma associated with cerebellar removal and isolation.

Alternatively some cells might have an abberant dendritic geometry, but this possibility could not be tested due to the small sample of such neurones that were also successfully filled with HRP. It is unlikely that the axons of Purkinje cells were significantly polarized by the applied current since, upon leaving the cell, they immediately enter a fibre bundle that lies perpendicular to the applied field. Likewise the mossy and climbing fibres mainly course in the same plane; the ascending portion of the climbing fibre might be polarized but we know little about the vertical extent of this afferent.

Due to the length of the vertical component, the parallel fibres and their parent granule cells might be significantly polarized. As will be shown below, the maximum depolarization that could be induced in an ascending parallel fibre by an applied field E is λE, where λ is the space constant. Since the diameter of a parallel fibre is less than 1 μm, λ is much smaller than that of dendritic cable structures and the amount of depolarization correspondingly less, for a given field. This argument was given added credibility in the experiments where the cerebellum was superfused with Ringer solution containing low-Ca^{2+} Ringer solution and 1 mM-Mn^{2+}. Under these conditions the modulation by applied field was not blocked or greatly changed, even though loc.-evoked spiking and the late component of field response, presumably representing post-synaptic depolarization, was abolished (Fig. 6 E–H). These results suggest that enhancement of excitatory synaptic input pathways was not a signficant mechanism contributing to the over-all modulation pattern in Purkinje cells. Thus it seems likely that the major element modulated was indeed the Purkinje cell itself.

Despite the apparent simplicity of the results, some issues remain puzzling. A major question is the nature of the spikes recorded. Since it has been conclusively established in other species (Llinás & Sugimori, 1980 a, b) that Purkinje cells generate calcium-mediated spikes in the dendrite and sodium-mediated spikes in the soma, it might be anticipated that calcium spikes would occur on the phase of pia-directed current (dendritic depolarization) and sodium spikes on the ventricle-directed current (somatic depolarization). This pattern could manifest itself as firing on both phases of the current (V/P modulation) if the recording were made at the soma and the calcium spikes were able to activate this region. This was rarely seen suggesting either that calcium spikes were unable to propagate to the soma, or unable to excite sodium spikes there, both possibilities being due to the hyperpolarization of the soma at the time for dendritic depolarization. If calcium spikes were generated in the dendrites

they should be recorded from those elements classified as distal Purkinje cell dendrites. These elements responded on the same current phase as the somatic and proximal dendritic units, however.

Further evidence against the spikes being generated by calcium currents in the range of field strength used in this study derives from the fact that the extracellular spikes were generally indistinguishable from those at the soma (except for very superficial elements where the amplitude was diminished). Detailed analysis of the recordings showed that most units ascribed to the soma or proximal dendritic group were recorded at a depth of 450–550 μm (median depth 500 μm) while the majority of distal dendritic elements were recorded between 250 and 400 μm (median depth 320 μm). A few units were recorded much more superficially and of these three were penetrated and identified as Purkinje cells (at 75, 150 and 230 μm). Histological examination of the sectioned material (with allowance for shrinkage) indicated that the average depth of Purkinje cell somata was in the range 400–500 μm.

Finally, our data indicate that the V modulation pattern recorded from Purkinje dendrites could be completely blocked by 1 μM-TTX. Taken in conjunction with the other criteria detailed above these results strongly suggest that the spikes that we recorded were mediated by sodium currents. Indeed, preliminary data (C. Y. Chan, J. Hounsgaard & C. Nicholson, unpublished observations) from a study using intra-cellular recording during field application showed that the threshold for activation of presumed calcium spikes was 2–4 times higher than that for presumed sodium spikes at any part of the Purkinje cell, and was usually greater than the maximum field strength used in the present study. The fact that the presumed sodium spikes were recorded extracellularly, at various dendritic levels does not demonstrate that they were generated there. In common with other Purkinje cells (Llinás & Sugimori, 1980 *a, b*) it is likely that the sodium spikes originated in the axon hillock, soma or possibly proximal dendrite and then electrotonically injected current into more distal dendritic regions. Detailed analysis of such mechanisms can only be made with intracellular recording, however.

Modulation of stellate cells

As described in the Results sections, stellate cells were divided into three groups based on the depth at which they were encountered. The modulation patterns differed significantly among the groups.

Table 1 and Fig. 11 show that the deepest stellates, recorded between 400 and 500 μm, were predominantly V modulated. From the population recorded, nineteen out of thirty-two (59%) showed this pattern, a similar proportion to the units encountered in the distal Purkinje cell dendrites. It was also evident from the histology that these deep-lying stellates usually had a dendritic tree with the dendrites oriented toward the pia like those of the Purkinje cells (Fig. 8*C, F*).

Of the m.m.s., only 35% (seven out of twenty) showed V modulation. This remained the largest single modulation class since six units in this population were non-modulated. Nevertheless, it is evident (see Table 1) that the modulation patterns are more diverse in this group than any of the others encountered up to this point. This finding can also be accounted for on the basis of geometry because in the mid-molecular layer (200–400 μm) the dendritic orientation tended to be diverse with some cells

showing a predominantly vertical orientation with the soma at the lower pole of the cell (Fig. 9*A*), others more horizontally oriented (Fig. 9*G*) and others having a more characteristic 'stellate' morphology with processes in many directions (Fig. 9*D*). It is noteworthy that of the three cells depicted in Fig. 9, only the vertically polarized cell showed V modulation.

Finally the u.m.s. showed no dominant modulation pattern. In fact the majority were not modulated (nine out of sixteen) and only one was V modulated. These cells lay in the upper 200 μm of the molecular layer and were the most difficult to locate so that the sample size was smaller than the other groups; nevertheless the modulation characteristics seem clear. Again modulation seems linked to dendritic morphology. Stellate cells at this level seem predominantly horizontally polarized (Fig. 10*C*, *E*).

Thus the modulation patterns of the stellate cells seem linked to the geometry of the dendrites. In particular only those groups having a strong vertical polarization of the dendrites with the soma at the lower pole were usually V modulated. One may ask whether we had a sufficient anatomical sample, given that we were dependent on HRP staining for revealing the dendritic pattern. We also had several series of material stained according to various Golgi methods that confirmed the general pattern of stellate cells that we have discussed (C. Nicholson, unpublished observations). In particular this latter histological material confirmed the diversity present amongst the m.m.s. In addition, the literature on stellate morphology in the rat describes one major orientation of dendrites in superficial stellate cells as largely horizontal. The rest of these cells show a more complicated pattern which conforms to neither 'stellate' nor vertical dendritic orientation (Palay & Chan-Palay, 1974).

Stellate cell–Purkinje cell interactions

Stellate cells are inhibitory interneurones in the cerebellum (Eccles, Llinás & Sasaki, 1966*a*). In the turtle, loc.-evoked responses of Purkinje cells were usually reduced by another closely preceding loc. stimulation, probably due to the inhibitory input from activated stellates onto the Purkinje cells. However, this effect was much less marked than in the mammal (Eccles *et al.* 1966*b*) or alligator (Llinás & Nicholson, 1969).

During field stimulation, both Purkinje cells and stellate cells were largely V modulated, which implied that the activation of Purkinje cells at the V phase could not be mediated through field-evoked reduction of tonic inhibitory input from the stellates. This supports the idea that Purkinje cells were predominantly modulated by direct field-induced polarization of their membranes. It is, however, possible that stellate cells act to reduce the modulation of Purkinje cells by virtue of their synchronous inhibition of the dendrites of the latter.

Threshold for modulation

Table 1 shows that of the units modulated, the mean values of the necessary field in each group lay between 15 and 20 mV/mm. These levels were typical of individual modulation classes as well with the possible exception of the P-modulated units which tended to have a lower threshold.

This uniformity is remarkable in that it encompasses two diverse types of cell

groups and subgroups within one of these types. When comparisons are made with other reports, however, the unanimity is even more striking. Thus Jefferys (1981) reported a threshold of 5–10 mV/mm for granule cells of the hippocampal slice. Amongst the older literature, Purpura & McMurtry (1965) estimated a threshold of 30–300 mV/mm for neurones of the motor cortex, as revealed by intracellular recording. As the authors admitted this latter value is subject to considerable error
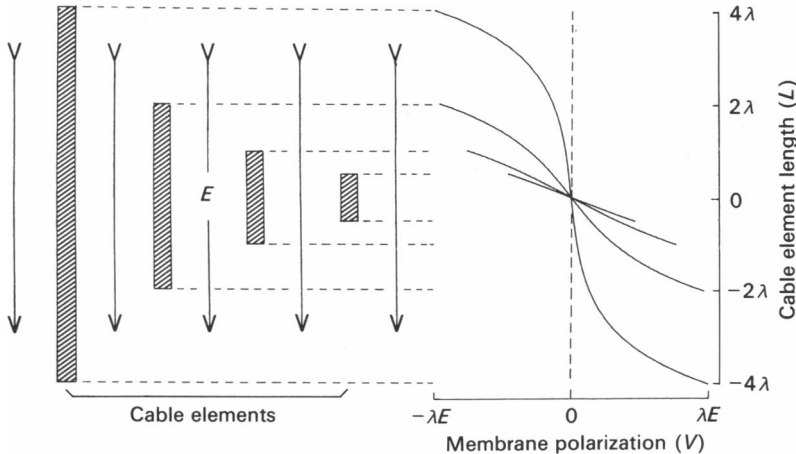

Fig. 12. Modulation of simple model cable element by applied electric field. Finite cable elements, sealed at both ends and characterized by space constants and variable length *L* are subject to a constant electric field *E*, parallel to their axes. The membrane polarizations (deviation of transmembrane potential from resting value), *V*, are indicated. Negative values represent hyperpolarization, positive values, depolarization. Further details in text.

due to field non-linearity in the tissue. In the crayfish stretch receptor, Terzuolo & Bullock (1956) reported a threshold of 1 mV/mm for modulation of active neurones and over 20 mV/mm for activation of inactive neurones.

Simple model of neuronal polarization

The simplest model consistent with our findings is that of a finite cable element subject to a constant field in the direction of its longitudinal axis (Fig. 12). Since many dendritic trees can be approximated to some degree by a single cable (Rall, 1977) this model is not unrealistic. The soma may either lie at the mid-point (a true 'stellate' cell) or at the lower extremity of the cable. Both ends of the element are assumed sealed; this implies negligible current flow into the axon.

Such a model as the one described has been studied previously (Sten–Knudsen, 1960; Ranck, 1963). For a cable of length $2L$ the polarization, V (i.e. the deviation of the transmembrane potential from its resting value) induced by a constant field E may be written as:

$$V = \lambda E \sinh (x/\lambda - L/\lambda)/\cosh (L/\lambda),$$

where λ is the space constant defined by $\lambda = \sqrt{(R_m/R_i)}$, where R_m is the membrane

resistance per unit area and R_i the intracellular axial resistance per unit length of the cable element. The distance coordinate x is measured from one end of the element.

The maximum polarization (V_{max}) is attained at the ends of the elements ($x = 0, 2L$) where $|V_{max}| = E \tanh (L/\lambda)$. As noted by Ranck (1975), this expression tends to λE for $L \gg \lambda$ and to LE for $L \ll \lambda$. Thus when the length of the element significantly exceeds the space constant, the maximum polarization approaches a constant value λE. For $\lambda = 250 \,\mu m$ and $E = 20 \, mV/mm$ this value is 5 mV. In contrast, when the element is much shorter than λ, the polarization is less and linearly related to the length. These features are illustrated in Fig. 12. The Figure shows that as the element lengthens, the polarization is concentrated near the end. Polarization is always symmetrical with hyperpolarization at the upper end and depolarization at the lower (for the indicated field direction).

Fig. 12 also demonstrates that cells such as Purkinje cells or l.m.s. will be maximally depolarized because their somata lie at the lowest point of the equivalent cable structure. Those m.m.s. which conform to a 'stellate' geometry and u.m.s. will tend to be unpolarized at the soma because it lies at the centre of symmetry. Since the majority of the u.m.s. have most of their processes in the horizontal direction, the equivalent cable element in the direction of the applied field is very short and even the extremities of the dendrites may be expected to undergo little polarization.

Conclusions

Our results demonstrate that amongst the Purkinje and stellate cells of the cerebellum the major determinant of modulation is orientation of dendrites and that when cells are oriented so that the soma is depolarized by the current they tend to be excited. Current flow in the opposite direction tends to inhibit them.

The similarities of the thresholds amongst cell types in this and other studies suggests that many cells can be modulated by fields of the order of 10–20 mV/mm provided that the dendritic geometry is suitably aligned with the applied field. This result is relevant to questions of ephaptic and field-mediated convulsive activity (Purpura, 1969; Snow & Dudek, 1984; Taylor *et al.* 1984). It is generally held that the amplitude of extracellular fields generated during brain seizure is between 4 and 20 mV/mm (see Jefferys, 1981).

Our studies also indicate the utility of this relatively simple stimulation method that enables populations of cells to be stimulated without penetration of individual cells. Moreover the current density is quite low at any point in the tissue since the current is not delivered by a local punctate electrode. A low-frequency sine wave both eliminates large capacitive membrane currents and permits phase relationships between stimulus and response to be defined. Such a stimulus is potentially valuable in prosthetic devices.

<div align="center">APPENDIX</div>

The cerebellum of the turtle may be approximated as an oblate spheroid with semi-major axes of length a, b and c. We assume that the axis of length c is oriented in the vertical or z-direction and that the other two orthogonal axes are equal and satisfy the relation $a = b > c$.

If a constant current J is applied parallel to the z-axis, and the conductivity of

the cerebellum is σ_c while that of the surrounding medium, i.e. the Ringer solution, is σ_m, then the situation is formally equivalent to an ellipsoid of one dielectric constant immersed in another and subject to a constant applied electric field (Stratton, 1941, pp. 207–217). This theory has been applied to the case of an ellipsoidal cell by Klee & Plonsey (1976). Based on these formulations, we can derive the following expressions:

Define $k = \sigma_c/\sigma_m$, then from Stratton (1941, pp. 211–212) we can write:

$$\phi_c(z) = \phi_0(z)/[1 + a^2 c(k-1)\, A/2],$$

where $\phi_0(z)$ is the potential induced by the applied current, J, in the absence of the cerebellum and $\phi(z)$ is the potential in the cerebellum. A is defined by the integral:

$$A = \int_0^\infty [(S+c^2)\, R]^{-1}\, \mathrm{d}S \quad \text{where} \quad R = (S+a^2)\,\sqrt{(S+c^2)},$$

where R and S are dummy variables.

This integral can be evaluated (Korn & Korn, 1968; p. 940, integral 138 and p. 939, integral 127) and we finally obtain the expression:

$$\phi_c(z) = -E_0 z H(k,u), \tag{A 1}$$

where

$$H(k,u) = [1 - (k-1)\,(1+u^2)\,(u\pi/2 - 1 - u\,.\,\arctan(u)]^{-1},$$

and $u = 1/\sqrt{(a^2/c^2 - 1)}$.

The term $(-E_0 z)$ is simply $\phi_0(z)$, the potential in the absence of the cerebellum and it also follows that $E_0 = J/\sigma_m$ where J is the applied current.

Since the field intensity in the cerebellum is, by definition, $-\partial\phi_c/\partial z$, it follows that this is $E_0 H(k,u)$ which is a constant. This remarkable fact was pointed out by Stratton (1941) and in fact is true for any arbitrarily oriented constant field applied to a conducting ellipsoid.

If we know $\epsilon = E_c/E_0$, and u, then from eqn. (A 1) we can derive an expression for k:

$$k = 1 + (1 - 1/\epsilon)\,[(1+u^2)\,(u\pi/2 - 1 - u\,.\,\arctan(u)]^{-1}. \tag{A 2}$$

Using expression 38 from Stratton (1941) we can derive the expression for the potential outside the cerebellum, $\phi_m(z)$ as:

$$\phi_m(z) = -E_0 H(k,u)\, f(k,u,c,z), \tag{A 3}$$

where

$$f = 1 + (k-1)\,(1+u^2)\,[c/z - 1 + u(\arctan(uz/c)) - \arctan(u)].$$

Note that in this case the factor $H(k,u)$ again appears but the additional term $f(k,u,c,z)$ is present and this latter term is a function of z.

REFERENCES

ARVANITAKI, A. (1942). Effects evoked in an axon by the activity of a contiguous one. *Journal of Neurophysiology* **5**, 89–108.

BAWIN, S. M., SHEPPARD, A. R., MAHONEY, M. D. & ADEY, W. R. (1984). Influences of sinusoidal electric evoked fields on excitability in the rat hippocampal slice. *Brain Research* **323**, 227–237.

BRINDLEY, G. S. & LEWIN, W. S. (1968). The visual sensations produced by electrical stimulation of the visual cortex. *Journal of Physiology* **196**, 479–493.

BROOKHART, J. M. & BLACHLY, P. H. (1952). Cerebellar unit responses to D.C. polarization. *American Journal of Physiology* **171**, 711.

DENNEY, D. & BROOKHART, J. M. (1962). The effects of applied polarization on evoked electrocortical waves in the cat. *Electroencephalography and Clinical Neurophysiology* **14**, 885–897.

ECCLES, J. C., ITO, M. & SZENTAGOTHAI, J. (1967). *The Cerebellum as a Neuronal Machine*. Berlin, Heidelberg, New York: Springer-Verlag.

ECCLES, J. C., LLINÁS, R. & SASAKI, K. (1966a). The inhibitory interneurones within the cerebellar cortex. *Experimental Brain Research* **1**, 1–16.

ECCLES, J. C., LLINÁS, R. & SASAKI, K. (1966b). Parallel fibre stimulation and the responses induced thereby in the Purkinje cells of the cerebellum. *Experimental Brain Research* **1**, 17–39.

FABER, D. S. & KORN, H. (1973). A neuronal inhibition mediated electrically. *Science* **179**, 577–578.

FURUKAWA, T. & FURSHPAN, E. J. (1963). Two inhibitory mechanisms in the Mauthner neurones of goldfish. *Journal of Neurophysiology* **24**, 140–176.

GARDNER-MEDWIN, A. R. (1983). Analysis of potassium dynamics in mammalian brain tissue. *Journal of Physiology* **335**, 393–426.

GARDNER-MEDWIN, A. R. & NICHOLSON, C. (1983). Changes of extracellular potassium activity induced by electric current through brain tissue in the rat. *Journal of Physiology* **335**, 375–392.

HAAS, H. L. & JEFFERYS, J. G. R. (1984). Low-calcium field burst discharges of CA1 pyramidal neurones in rat hippocampal slices. *Journal of Physiology* **354**, 185–201.

JEFFERYS, J. G. R. (1981). Influence of electric fields on the excitability of granule cells in guinea-pig hippocampal slices. *Journal of Physiology* **319**, 143–152.

JEFFERYS, J. G. R. & HAAS, H. L. (1982). Sychronized bursting of CA1 hippocampal pyramidal cells in the absence of synaptic transmission. *Nature* **300**, 448–450.

KATZ, B. & SCHMITT, O. H. (1940). Electrical interaction between two adjacent nerve fibres. *Journal of Physiology* **97**, 471–488.

KLEE, M. & PLONSEY, R. (1976). Stimulation of spheroidal cells – the role of cell shape. *Institute of Electrical and Electronic Engineers. Transactions in Biomedical Engineering* **23**, 347–354.

KORN, H. & AXELRAD, H. (1980). Electrical inhibition of Purkinje cells in the cerebellum of the rat. *Proceedings of the National Academy of Sciences of the U.S.A.* **77**, 6244–6247.

KORN, H. & FABER, D. S. (1975). An electrically mediated inhibition in goldfish medulla. *Journal of Neurophysiology* **38**, 452–471.

KORN, G. A. & KORN, T. M. (1968). *Mathematical Handbook for Scientists and Engineers*. New York: McGraw-Hill.

LANDAU, W. M., BISHOP, G. H. & CLAIRE, M. H. (1965). Site of excitation in stimulation of the motor cortex. *Journal of Neurophysiology* **28**, 1206–1222.

LLINÁS, R. (1976). Cerebellar Physiology. In *Frog Neurobiology. A Handbook*, ed. LLINÁS, R. & PRECHT, W., pp. 892–923. Berlin: Springer-Verlag.

LLINÁS, R. & HILLMAN, D. E. (1969). Physiological and morphological organization of the cerebellar circuits in various vertebrates. In *Neurobiology of Cerebellar Evolution and Development*, ed. LLINÁS, R., pp. 43–77. Chicago: American Medical Association, Education and Research Foundation.

LLINÁS, R. & NICHOLSON, C. (1969). Electrophysiological analysis of alligator cerebellar cortex: A study on dendritic spikes. In *Neurobiology of Cerebellar Evolution and Development*, ed. LLINÁS, R., pp. 431–465. Chicago: American Medical Association, Education and Research Foundation.

LLINÁS, R. & SUGIMORI, M. (1980a). Electrophysiological properties of *in vitro* Purkinje cell somata in mammalian cerebellar slices. *Journal of Physiology* **305**, 171–195.

LLINÁS, R. & SUGIMORI, M. (1980b). Electrophysiological properties of *in vitro* Purkinje cell dendrites in mammalian cerebellar slices. *Journal of Physiology* **305**, 197–213.

LUTZ, P. L., LAMANNA, J. C., ADAMS, M. R. & ROSENTHAL, M. (1980). Cerebral resistance to anoxia in the marine turtle. *Respiration Physiology* **41**, 241–251.

NICHOLSON, C. & FREEMAN, J. A. (1975). Theory of current source-density analysis and determination of conductivity tensor for anuran cerebellum. *Journal of Neurophysiology* **38**, 356–368.

NICHOLSON, C. & HOUNSGAARD, J. (1983). Diffusion in the slice microenvironment and implications for physiological studies. *Federation Proceedings* **42**, 2865–2868.

NICHOLSON, C., LLINÁS, R. & PRECHT, W. (1969). Neural elements of the cerebellum in elasmobranch fishes: Structural and functional characteristics. In *Neurobiology of Cerebellar Evolution and Development*, ed. LLINÁS, R., pp. 215–243. Chicago: American Medical Association, Education and Research Foundation.

NICHOLSON, C. & PHILLIPS, J. M. (1981). Ion diffusion modified by tortuosity and volume fraction in the extracellular microenvironment of the rat cerebellum. *Journal of Physiology* **321**, 225–257.

PALAY, S. L. & CHAN-PALAY, V. (1974). *Cerebellar Cortex, Cytology and Organization*, pp. 216–233. New York, Heidelberg, Berlin: Springer-Verlag.

PURPURA, D. P. (1969). Mechanisms of propagation: Intracellular studies. In *Basic Mechanisms of the Epilepsies*, ed. JASPER, H. H., WARD, A. A. & POPE, A., pp. 441–451. London: Little Brown.

PURPURA, D. P. & McMURTRY, J. G. (1965). Intracellular activities and evoked potential changes during polarization of motor cortex. *Journal of Neurophysiology* **28**, 166–185.

PURPURA, D. P. & MALLIANI, A. (1966). Spike generation and propagation initiated in dendrites by trans-hippocampal polarization. *Brain Research* **1**, 403–406.

RALL, W. (1977). Core conductor theory and cable properties of neurones. In *Handbook of Physiology: The Nervous System*, section 1, vol. 1, ed. BROOKHART, J. M. & MOUNTCASTLE, V. B., pp. 39–97. Bethesda: American Physiological Society.

RANCK JR, J. B. (1963). Analysis of specific impedance of rabbit cerebral cortex. *Experimental Neurology* **7**, 153–174.

RANCK JR, J. B. (1975). Which elements are excited in electrical stimulation of mammalian cerebral nervous system: A review. *Brain Research* **98**, 417–440.

SNOW, R. W. & DUDEK, F. E. (1984). Electrical fields directly contribute to action potential synchronization during convulsant-induced epileptiform bursts. *Brain Research* **323**, 114–118.

STEIN-KNUDSEN, O. (1960). Is muscle contraction initiated by internal current flow? *Journal of Physiology* **151**, 363–384.

STRATTON, J. A. (1941). *Electromagnetic Theory*. New York: McGraw-Hill.

TAYLOR, C. P. & DUDEK, F. E. (1984*a*). Excitation of hippocampal pyramidal cells by an electrical field effect. *Journal of Neurophysiology* **52**, 126–142.

TAYLOR, C. P. & DUDEK, F. E. (1984*b*). Synchronization without active chemical synapses during hippocampal afterdischarges. *Journal of Neurophysiology* **52**, 143–155.

TAYLOR, C. P., KRNJEVIĆ, K. & ROPERT, N.(1984). Facilitation of hippocampal CA3 pyramidal cell firing by electrical fields generated antidromically. *Neuroscience* **11**, 101–109.

TERZUOLO, C. A. & BULLOCK, T. H. (1956). Measurement of imposed voltage gradient adequate to moderate neuronal firing. *Proceedings of the National Academy of Sciences of the U.S.A.* **42**, 687–694.

YEDLIN, M., KWAN, H., MURPHY, J. T., NGUYEN-HUU, H. & WONG, Y. C. (1974). Electrical conductivity in cat cerebellar cortex. *Experimental Neurology* **43**, 555–569.